
HANDLING LABEL NOISE VIA INSTANCE-LEVEL DIFFICULTY MODELING AND DYNAMIC OPTIMIZATION

Kuan Zhang

Beijing Institute of Technology
zhangkuan@bit.edu.cn

Chengliang Chai

Beijing Institute of Technology
ccl@bit.edu.cn

Jingzhe Xu

Beijing Institute of Technology
xjz@bit.edu.cn

Chi Zhang

Beijing Institute of Technology
zc315@bit.edu.cn

Ye Yuan

Beijing Institute of Technology
yuan-ye@bit.edu.cn

Guoren Wang

Beijing Institute of Technology
wanggrbit@bit.edu.cn

Lei Cao

University of Arizona
lcao@csail.mit.edu

ABSTRACT

Recent studies indicate that deep neural networks degrade in generalization performance under noisy supervision. Existing methods focus on isolating clean subsets or correcting noisy labels, facing limitations such as high computational costs, heavy hyperparameter tuning process, and coarse-grained optimization. To address these challenges, we propose a novel two-stage noisy learning framework that enables instance-level optimization through a dynamically weighted loss function, avoiding hyperparameter tuning. To obtain stable and accurate information about noise modeling, we introduce a simple yet effective metric, termed *wrong event*, which dynamically models the cleanliness and difficulty of individual samples while maintaining computational costs. Our framework first collects *wrong event* information and builds a strong base model. Then we perform noise-robust training on the base model, using a probabilistic model to handle the *wrong event* information of samples. Experiments on five synthetic and real-world LNL benchmarks demonstrate our method surpasses state-of-the-art methods in performance, achieves a nearly 75% reduction in computational time and improves model scalability.

1 Introduction

Label noise is an unavoidable issue in training deep neural networks (DNNs), particularly when dealing with large-scale datasets annotated through web scraping [1], crowd-sourcing [2], or pre-trained models [3]. Apparently, label noise is likely to degrade the model performance [4], mainly because the model tends to fit the noise patterns. To be specific, recent studies have found that DNNs have the *memorization effect* [5], i.e., DNNs first learn clean patterns early in training, then start fitting noise later, and eventually overfit the noisy dataset.

To alleviate this problem, researchers have explored the use of *memorization effect* for the learning with noisy labels (LNL) task, which can be classified into three types of approaches, i.e., sample selection, loss regularization and label correction. Sample selection [6–8] leverages early-stage loss to identify clean samples for training, but it totally neglects the value of noisy data [9]. To address this, loss regularization methods [10, 11] model both clean and noisy samples by incorporating regularization terms or designing robust loss functions. However, they struggle in more challenging scenarios [12] like instance-dependent noise because they don’t fundamentally correct the noisy labels. Recent state-of-the-art approaches, label correction methods partition datasets into different subsets, such as the clean/noise set [13, 14] or clean/hard/noise set [12, 15]. Then they preserve the given labels in clean set and generate

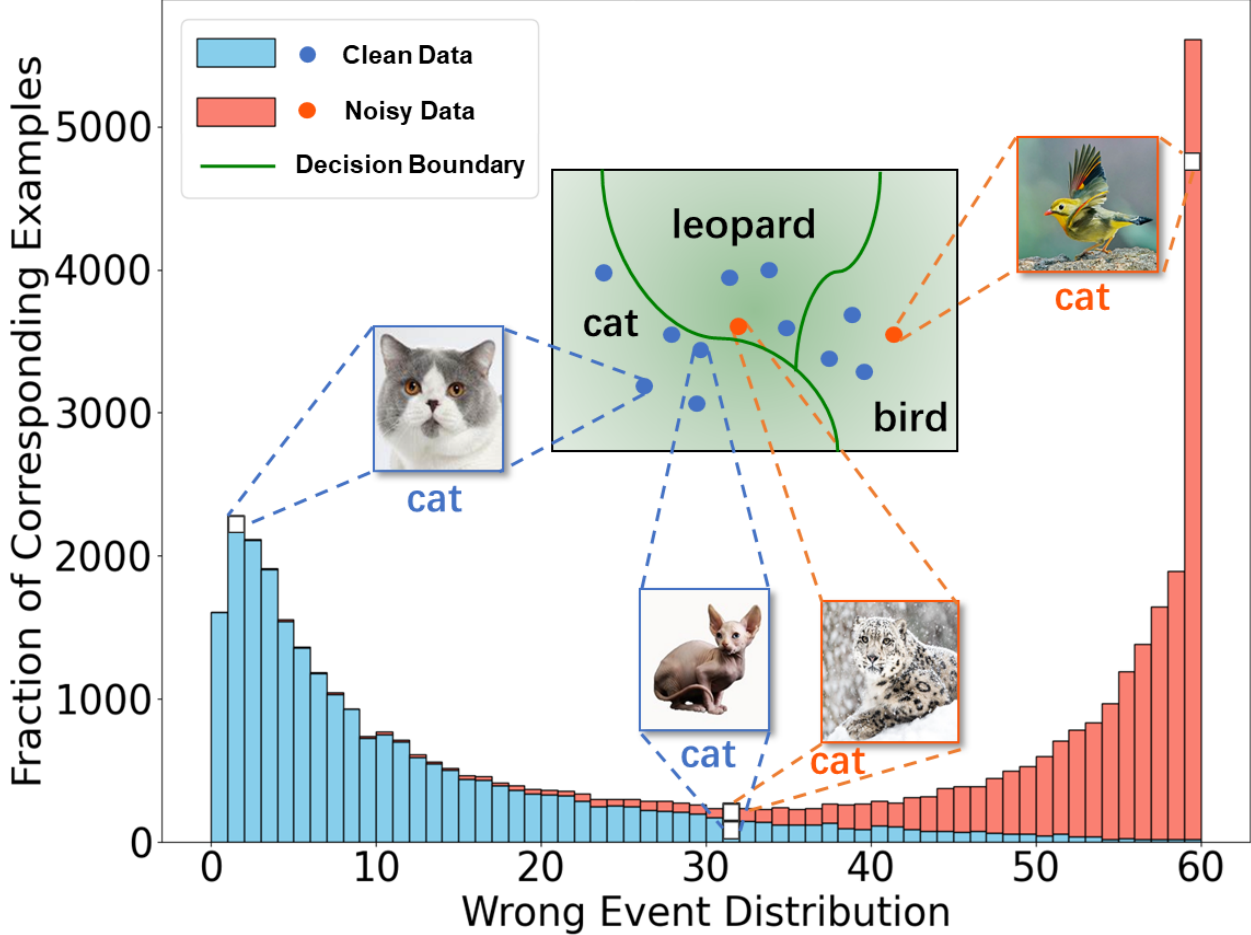


Figure 1: A bar chart is shown to illustrate the distribution of wrong events. From the perspective of noise, clean samples typically exhibit lower wrong event values, while noisy samples tend to have higher wrong event values. From the perspective of sample difficulty, samples located at the extremes of the distribution are far from the decision boundaries (e.g., cat and bird in the figure), exhibit typical features, and are classified with high confidence by the model, representing easy samples. In contrast, samples located in the central depression of the distribution are often near the decision boundaries of multiple classes (e.g., cat and leopard in the figure). These samples are classified with low confidence by the model and represent hard samples.

pseudo labels for noise set to achieve remarkable improvement. However, current label correction methods have the following limitations.

Limitations. (1) Accurate partitioning strategies are always computationally intensive such as co-training frameworks [6, 14, 16], k-means clustering [17] and contrastive loss [16]. (2) Exhaustive hyperparameter tuning is necessary such as coefficients of loss terms [10, 12, 14], filtering threshold to split subsets [6, 14, 16] and the warm-up period to obtain a model have not fitted the noise [9, 12, 14]. (3) Existing works [12, 14, 15] always assign identical coefficients to all samples in the same subset, neglecting individual differences in cleanliness and difficulty within each subset.

Our Proposal. To address these limitations, we propose **DODO**, an instance-level **D**ifficulty **M**odeling and **D**ynamic Optimization framework to achieve robust training over noisy data. The key idea is to design a dynamically weighted loss function that captures both the cleanliness and difficulty of each individual samples, enabling instance-level optimization. The loss function consists of three terms, i.e., clean, noise, and hard components. The weights for clean and noise components are dynamically adjusted based on sample cleanliness, while the weight of hard component is determined by sample difficulty, 25 indicating that model performance is highly correlated with the cleanliness and difficulty modeling.

To this end, we introduce a new noise-robust metric termed *wrong event*, which counts the frequency of mismatches between model predictions and given labels across all the epochs during training. This metric can effectively capture both the cleanliness and difficulty of each individual sample (see Fig.1), providing adaptive weights for the loss function.

Notably, *wrong event* achieves high computational efficiency while enabling accurate and robust modeling at any training stage (see Fig.2). By aggregating information across the entire training process, *wrong event* demonstrates superior stability in modeling hard and noisy samples, effectively avoiding the inaccurate subset partitioning frequently happened in loss-based modeling methods due to the loss mutation of hard and noisy samples [18].

Overall, DODO leverages *wrong event* as a key metric in a two-stage process (see Fig.3). In the first stage, we adopt a conventional training strategy to collect *wrong event* information for each sample and obtain a competitive base model. In the second stage, we perform robust training on the basis of the base model, so the training effectiveness is improved. More specifically, a two-component beta mixture model (BMM) is employed to fit the distribution of *wrong event*, providing dynamic weights for the loss function. This iterative process ensures that *wrong event* information and the model performance mutually benefit each other, leading to much improvement throughout the training process.

We summarize our main contributions as follows:

- We propose *wrong event*, a simple but effective metric that can reliably separate noisy samples from clean ones at any stage of training, even if the model is fitting noise. We provide detailed analysis to explain why *wrong event* works well.
- We propose DODO, a two-stage noisy learning framework based on *wrong event*. Specifically, we first collect *wrong event* information and obtain a good base model. Then, we continue to train a more robust model with a dynamically weighted loss using *wrong event* information.
- We run extensive experiments and show that DODO significant outperforms state-of-the-art methods by an average accuracy of 1.1% on synthetic and 0.8% on real-world datasets for LNL tasks, with a nearly 75% reduction in computational time, a better scalability to larger models compared to previous methods and without parameter tuning.

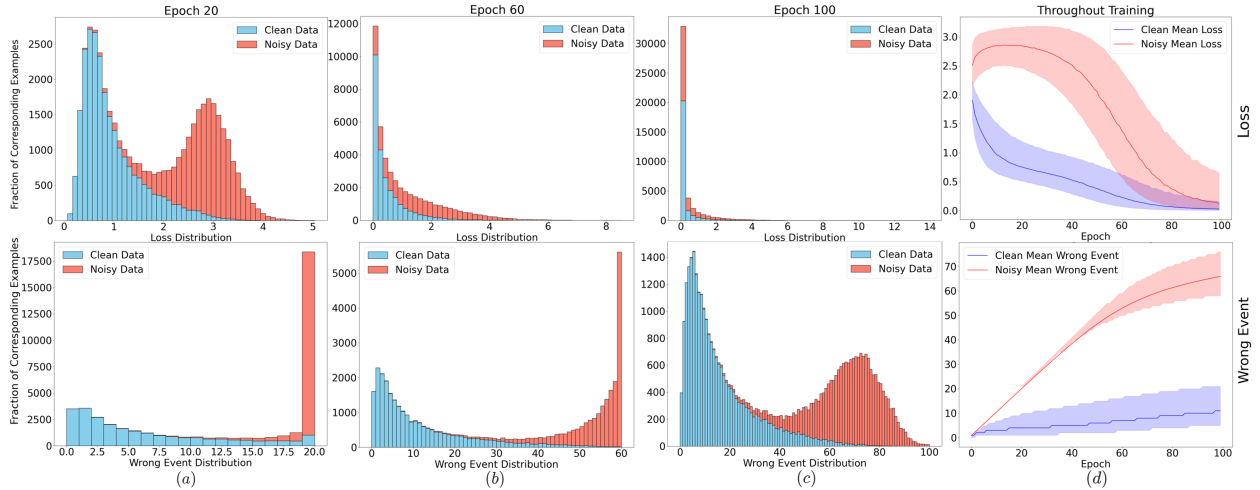


Figure 2: A comparison between wrong event and loss. The baseline model is ResNet-18 trained on CIFAR-10 with 50% symmetric noise for 100 epochs. We show the loss distributions (the first row) and wrong event distribution (the second row) during training. The four columns, (a) (b) (c) (d), represent the distributions at epoch 20, 60, 100 and the entire training phase. In (d), the heavy lines represent the median value and the shaded areas are the interquartile ranges, respectively. Since wrong events are monotonically increasing based on historical statistics instead of current model prediction, when model overfits the dataset, wrong event values for all samples do not change, rather than converging to zero as loss values typically do. As a result, wrong event can clearly separate noisy data and clean data in all training stages, even if the model fits noise.

2 Related Works

Memorization & Forgetting. [4] observe that DNNs are sufficient for memorizing the entire dataset. [5] propose that DNNs follow the *memorization effect*. Researchers have studied the phenomenon and proposed some metrics. [19] proposed *forgetting event*, which counts how many times a model forgets a prediction of given labels. However, the model tends to predict ground truth labels rather than the given noisy labels for easy noisy samples consistently, resulting in the value of zero in early stage. [20] proposed *first k-epoch learning*, i.e., a sample has been predicted to its

given label for consecutive k epochs for the first time. However, k is a hyperparameter which changes due to depending on the characteristics of the dataset. Though these metrics exhibit robustness during the model overfitting phase, their ability to distinguish between clean and noisy samples in the early stage is inferior to that of loss-based modeling. Our proposed *wrong event* metric demonstrates strong discriminative capabilities at all stages of model training, without long training periods.

Learning with Noise Labels (LNL). LNL problem has been extensively explored in recent research [8, 12, 21, 22]. There are many variants of the LNL problem. Some methods [23, 24] suppose the existence of a small subset of clean data, while we do not rely on such assumptions. Facing this more challenging scenario, recent studies applied many techniques, such as co-training frameworks [6, 14, 16], k-means clustering [17], and contrastive loss [16, 25], which require high computation and memory costs. To achieve instance-level optimization, dynamic loss functions are considered, but previous methods [9, 24] mainly focused on modeling clean and noisy samples dynamically, often overlooking the challenge of hard samples. Our simple yet robust *wrong event* modeling reduces computational costs, and the dynamic loss function simultaneously considers both sample cleanliness and difficulty.

Pre-trained Models for LNL. Pre-trained models are recognized for their strong generalization performance with fast adaptation [26, 27]. Previous studies [21, 28] incorporate SimCLR [29] and MoCo [30] for label-noise learning, by using self-supervised pre-trained methods. Recent LNL methods [8, 22, 31] leverage pre-trained vision foundation models such as ResNet [32], ViT [26], CLIP [27] and ConvNeXt [33] to improve effectiveness and efficiency. However, larger models restricts the application of complex modeling approaches [8, 22], so they primarily rely on simple strategies such as the small-loss criterion or similarity threshold to filter out clean subsets for training, neglecting the value of noisy data. Our approach utilizes both clean and noisy information across the complete dataset, due to the high efficiency of *wrong event*. By doing so, DODO achieves superior model performance while keeping high efficiency.

3 Preliminary and Initial Findings

In this section, we first introduce the problem setting of label noise learning. Subsequently, we formally define the concept of *wrong event* and present empirical evidence to demonstrate its robustness. Finally, we will discuss how to utilize the information provided by *wrong event*.

3.1 Settings of Noise Label Learning

In the context of a C -class image classification problem, we denote the training dataset as $D_{\text{train}} = \{(x_i, \bar{y}_i)\}_{i=1}^N$, which consists of N pairs of input images x_i and their given labels $\bar{y}_i \in \{1, \dots, C\}$. In real-world scenarios, the given labels \bar{y}_i may be corrupted due to various factors. We use y_i to represent the ground truth label of (x_i, \bar{y}_i) , which remains inaccessible during the training phase. It is widely acknowledged that models trained on noisy labeled datasets D_{train} using traditional cross-entropy loss often exhibit poor performance on clean test data. This limitation poses challenges when deploying models in real applications. Consequently, it becomes crucial to develop robust models capable of effectively handling datasets with noisy labels.

3.2 Observation of Wrong Event

We begin by formally defining the concept of *wrong event*. Consider a model $f(\cdot)$ with parameter θ trained over T epochs. For a given sample (x_i, \bar{y}_i) , the *wrong event* is computed as follows:

$$\text{wrong event}_i = \sum_{t=1}^T \mathbb{I}(f_t(x_i) \neq \bar{y}_i) \quad (1)$$

where $\mathbb{I}(\cdot)$ denotes the indicator function. This metric quantifies the cumulative number of epochs in which the model's prediction $f(x_i)$ disagrees with the given label \bar{y}_i . Based on empirical observations (See Fig.2), we found that *wrong event* can reliably separate noisy samples from clean samples at any stage of training, even if the model fits noise. We conduct extensive experiments to verify that *wrong event* is a more robust and informative metric than loss in more challenging noisy scenarios (see Appendix C) and provides more accurate modeling than other metrics (see Table 4). Before diving into the explanations behind this phenomenon, we need to make some definitions. *Easy samples* are those that lie far from the decision boundary, while *hard samples* are those located near the decision boundary. According to the widely accepted perspective in LNL [4, 34], the model should prioritize fitting samples in the following order: (1) *easy clean samples*, (2) *hard samples* (which can be either clean or noisy), and (3) *easy noisy samples*.

We consider three explanations behind this phenomenon. **1) Prediction itself is a dynamic threshold.** The model's judgement can be likened to a dynamic threshold that adapts based on the characteristics of the data and the training

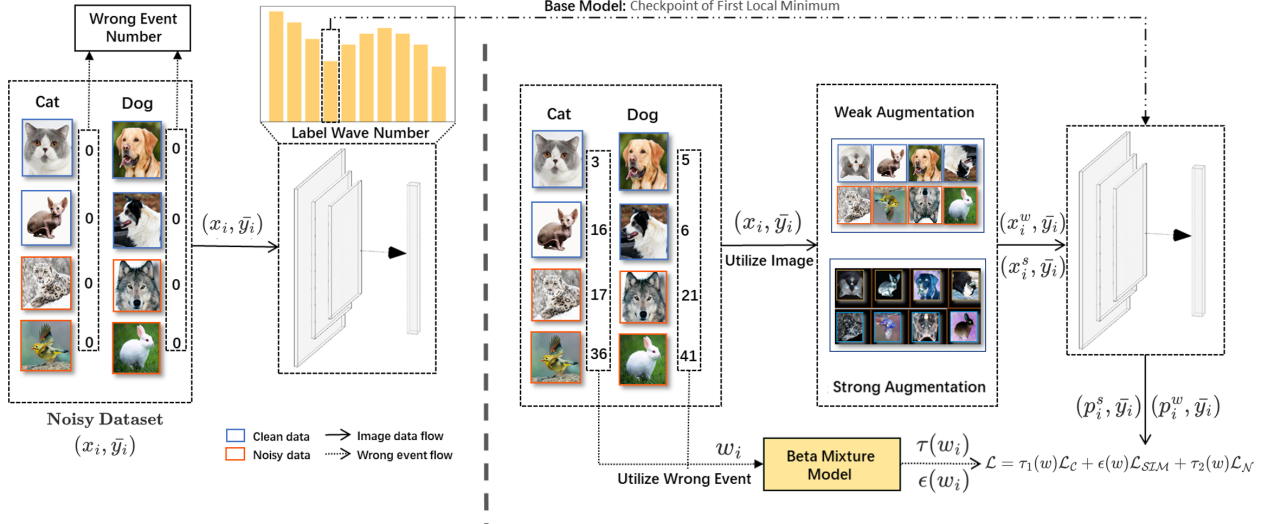


Figure 3: Illustration of the proposed DODO framework. The training process is divided into two stages. In the first stage, prior knowledge, i.e., coarse distribution of wrong event, is obtained, and a base model that owns basic discrimination capability is captured. In the second stage, robust noise learning is performed. By using BMM, we obtain both cleanliness and difficulty information for individual samples, enabling instance-level dynamic optimization. The sample’s wrong event information and the model’s classification capability mutually benefit each other, leading to much improvement.

progress. Unlike predefined thresholds that often require adjustments based on noise rates and noise types, *wrong event* leverages the model’s inherent learning dynamics, eliminating the need for hyperparameter tuning. To some extent, the wrong event maps the loss values to 0 or 1 based on a confidence-dependent dynamic threshold, where lower (higher) loss values are more likely to be mapped to 0 (1). **2) Wrong event is robust to noise.** The variation of *wrong event* across consecutive epochs is significantly smaller compared to that of loss values. Specifically, while the loss of hard or noisy samples has been empirically observed to exhibit substantial fluctuations between two consecutive epochs [18], *wrong event* remains either unchanged or increases by at most 1 in the same interval. This stability stems from the fact that *wrong event* is a cumulative metric, reflecting the model’s historical prediction errors rather than instantaneous performance. Even if the model overfits to a noisy dataset, the outcome is simply that the *wrong event* values for all samples remain constant, rather than converging to zero as loss values typically do. **3) Wrong event reflects cleanliness and difficulty.** *Easy samples*, which are located far from the decision boundary, exhibit consistent prediction behavior across consecutive epochs: clean(noisy) samples are consistently predicted correctly(incorrectly). As a result, these samples tend to occupy the extremes of the *wrong event* distribution. In contrast, *hard samples*, which lie close to the decision boundary, often experience fluctuating predictions, with their outcomes frequently flipping between similar classes. This instability causes hard samples to cluster in the middle region of the *wrong event* distribution, forming a low-lying trough. The distribution of *wrong event* provides valuable insights into both the cleanliness and the difficulty of each sample.

3.3 Utilize Wrong Event

In the context of LNL, probabilistic models are frequently employed to characterize the noise distribution. The two-component Gaussian mixture model (GMM) is commonly used to distinguish clean samples from noisy ones, and a threshold-based approach is employed to partition the dataset into different subsets [14, 16]. In all following equations, the symbol w is used to denote the *wrong event*. The probability density function (pdf) of a mixture model of two components on *wrong event* is defined as:

$$p(w) = \sum_{k=1}^2 m_k \cdot p(w|k) \quad (2)$$

where m_k are the mixing coefficients for the convex combination of each individual pdf $p(w|k)$. In our case, *wrong event* of easy samples, especially easy noisy samples, often concentrate at the distribution tails, leading to a monotonically increasing rather than unimodal distribution (see Fig.1,2). This phenomenon can be attributed to three main factors: **1) Hard samples** [35, 36] often exhibit a long-tailed distribution in training; **2) Curriculum learning** [37] suggests that

models learn easy samples quickly but struggle with hard samples; 3) Training typically stops before the model fully memorizes the dataset, leading to an accumulation of easy noisy samples in the tail of the noise distribution.

These characteristics make Gaussian distribution models inadequate for fitting. To better model such distributions, we adopt a two-component beta mixture model (BMM), which is well-suited for capturing both symmetric, skewed and monotonically increasing distributions over $[0, 1]$ due to the flexibility of the beta distribution [38]. The beta distribution over a (max) normalized *wrong event* $\in [0, 1]$ is defined to have pdf:

$$B(\alpha, \beta) = \frac{\Gamma(\alpha)\Gamma(\beta)}{\Gamma(\alpha + \beta)} \quad (3)$$

$$p(w|\alpha, \beta) = \frac{w^{\alpha-1} \cdot (1-w)^{\beta-1}}{B(\alpha, \beta)} \quad (4)$$

where $\alpha, \beta > 0$ and $\Gamma(\cdot)$ is the Gamma function, and the mixture pdf is given by substituting the above into Eq. 2. We use an Expectation Maximization (EM) procedure to fit the BMM to the observations [9, 14]. Specifically, we introduce two variables:

$$\tau_k(w) = p(k|w) = \frac{p(k) \cdot p(w|k)}{p(w)} \quad (5)$$

which defines the posterior probability of the given *wrong event* having been generated by mixture component k ,

$$\lambda_k(w) = F(w; \alpha_k, \beta_k) = \frac{\int_0^w t^{\alpha_k-1} (1-t)^{\beta_k-1} dt}{B(\alpha_k, \beta_k)} \quad (6)$$

which defines the cumulative distribution function (CDF) value of a beta mixture component k for a given *wrong event*.

The fitting process yielded two beta distributions, \mathcal{B}_1 and \mathcal{B}_2 , with means μ_1 and μ_2 (assuming that μ_1 is smaller than μ_2). We need to utilize \mathcal{B}_1 and \mathcal{B}_2 to measure the cleanliness and difficulty of the samples. 1) **Cleanliness**. We associate \mathcal{B}_1 with the clean distribution for lower mean, as it captures the characteristics of correctly labeled samples, while \mathcal{B}_2 is attributed to the noisy distribution, representing mislabeled samples. Thus, $\tau_1(\cdot)$ corresponds to the probability of a sample being drawn from the clean distribution, while $\tau_2(\cdot) = 1 - \tau_1(\cdot)$ represents the probability of a sample originating from the noisy distribution. 2) **Difficulty**. In the clean distribution, samples with larger *wrong event* values tend to be closer to the decision boundary. Conversely, in the noisy distribution, samples with smaller *wrong event* values are closer to the decision boundary. We use posterior probabilities $\tau(\cdot)$ and the cumulative distribution function $\lambda(\cdot)$ to measure the difficulty level of the samples:

$$\epsilon(w) = \tau_1(w) \cdot \lambda_1(w) + \tau_2(w) \cdot (1 - \lambda_2(w)) \quad (7)$$

where $\epsilon(w)$ represents the difficulty level of a sample with a given *wrong event*. The larger (smaller) $\epsilon(w)$ is, the closer (farther) the sample is to the decision boundary, indicating a higher (lower) difficulty level of the sample. It can be observed that when $w \rightarrow \min\{w_i\}_{i=1}^N$ or $\max\{w_i\}_{i=1}^N$, $\epsilon(w) \rightarrow 0$, and when $w \rightarrow \text{middle}$, $\epsilon(w) \rightarrow 1$.

Due to the heterogeneous distribution of *wrong event* across different classes—where simpler classes typically exhibit lower wrong event means compared to harder ones—fitting a single distribution to the entire dataset proves insufficiently precise. To achieve more accurate modeling and maintain class balance, we establish C BMM models to individually model the distribution of each class. For samples i where $\bar{y}_i = c$, the posterior probabilities are derived from the corresponding BMM components \mathcal{B}_1^c and \mathcal{B}_2^c , achieving more accurate and fine-grained modeling.

4 Robust Denoising Framework

Briefly speaking, prior knowledge, i.e., *wrong event* information and a competitive base model is obtained in the first stage, and this prior knowledge is utilized to build on the base model with continuous noise-robust training in the second stage.

4.1 Two Stage Training

Stage 1: Obtain prior knowledge. The first phase has two main objectives. Firstly, we adopted a typical training strategy, which involves training the model using the cross-entropy loss function for a certain period and collecting *wrong event* information.

$$\mathcal{L}_{ce}(x_i, \bar{y}) = -\bar{y} \log(f(x_i)) \quad (8)$$

Secondly, we aim to capture a competitive base model during training to serve as the initial model for stage 2, thereby improving training quality. Recent research [34] introduced a metric called *label wave*, which records the

number of prediction changes per epoch. The model at the first local minimum of prediction changes exhibits strong competitiveness in LNL settings. In particular, this technique does not increase the computational cost of DODO. Notably, multiple fine-tuning approaches can be employed in stage 1, including Linear Probing (LP) or Full Fine Tuning (FFT). For smaller models such as ResNet-50, we recommend using FFT to achieve a more competitive base model and improve the accuracy of *wrong event* estimation. For larger models such as ViT-B/16, we suggest using LP to accelerate training. The stage 1 process is illustrated in the left side of Fig.3.

Stage 2: Robust Model Adaptation. The second phase of the algorithm aims to train a noise-robust model based on the base model, incorporating prior knowledge. The overall training objective of second phase is:

$$\mathcal{L} = \sum_{i=1}^N [\gamma_1(w_i) \cdot \mathcal{L}_C + \epsilon(w_i) \cdot \mathcal{L}_{S\mathcal{I}\mathcal{M}} + \gamma_2(w_i) \cdot \mathcal{L}_N] \quad (9)$$

where $\tau_1(\cdot)$, $\tau_2(\cdot)$ are the posterior probabilities of \mathcal{B}_1 , \mathcal{B}_2 , and $\epsilon(\cdot)$ is the difficulty coefficient in Eq. 7. We will give the formation of each loss function in detail in the following subsection. After each epoch of robust training, we also update the *wrong event* information for each sample. With more accurate model output, the clean distribution and the noisy distribution gradually separate, providing the model with more accurate modeling. In this way, both the model and the *wrong event* information become more accurate. The stage 2 process is illustrated in the right side of Fig.3.

4.2 Analysis of Loss Function

For an instance x , two-view augmentation generates a weak view x^w and a strong view x^s [39, 40]. For clean distribution \mathcal{B}_1 , we utilize the typical cross-entropy loss for both views, leading to the loss term \mathcal{L}_C :

$$\mathcal{L}_C = \mathcal{L}_{ce}(x_i^w, \bar{y}) + \mathcal{L}_{ce}(x_i^s, \bar{y}) \quad (10)$$

where \mathcal{L}_{ce} is cross-entropy loss in Eq. 8. For noisy distribution \mathcal{B}_2 , we compute the linear average of the model outputs from the two views to obtain a robust pseudo-label to replace \bar{y} :

$$f(x_i) = \frac{1}{2}f(x_i^w) + \frac{1}{2}f(x_i^s) \quad (11)$$

which leads to the loss term \mathcal{L}_N :

$$\mathcal{L}_N = -f(x_i) \log(f(x_i)) \quad (12)$$

To optimize the difficult samples, we aim to enhance the feature extraction capability of the model for these samples, as their labels and model outputs are often inaccurate. Specifically, we encourage the outputs of the two views to be as close as possible, and we use $\mathcal{L}_{S\mathcal{I}\mathcal{M}}$ to measure this similarity:

$$\mathcal{L}_{S\mathcal{I}\mathcal{M}} = (f(x_i^w) - f(x_i^s))^2 \quad (13)$$

$\mathcal{L}_{S\mathcal{I}\mathcal{M}}$ is the mean squared error (MSE) between the two predictions. We use $\mathcal{L}_{S\mathcal{I}\mathcal{M}}$ to increase the loss weight for difficult samples, encouraging the model to focus more on learning from these samples and thereby achieving more robust feature extraction and classification capabilities.

5 Experiments

5.1 Experimental Settings

Synthetic Datasets. We begin by evaluating the performance of DODO on two image classification benchmarks using synthetic datasets with varying types and ratios of noisy labels. Specifically, we conducted experimental analyzes on the widely used CIFAR-100 [41] and Tiny-ImageNet [42] datasets. Given a noise transition matrix $T \in [0, 1]^{K \times K}$, where T_{ij} represents the probability of a ground-truth label i being flipped to a corrupted label $\bar{y} = j$. Following previous works [12, 22], we introduce three common types of label noise: **1) Symmetric Noise** [6, 14]: With noise rate η and a K -class image classification task, we define $T_{ij} = \frac{\eta}{K}$ for $i \neq j$, where the true labels are replaced with random labels. **2) Asymmetric Noise:** $T_{ij} = p(\bar{y} = j | y = i)$, which is designed to mimic the structure of real-world label noise. The labels are only replaced by similar classes. **3) Instance-dependent Noise:** $T_{ij} = p(\bar{y} = j | y = i, x)$, which represents a more realistic scenario that considers the influence of instance x in the label corruption process, such as the instance-dependent noise proposed in [43].

Following setting of previous work [8, 9, 25], we conduct extensive experiments on CIFAR-100 with symmetric noise ratio $r \in \{0.2, 0.4, 0.6\}$, asymmetric noise ratio $r \in \{0.4\}$ and instance-dependent noise ratio $r \in \{0.4\}$, and on Tiny-ImageNet with symmetric noise ratio $r \in \{0.2, 0.5\}$ and instance-dependent noise ratio $r \in \{0.4\}$.

Methods	Architecture	CIFAR-100					Tiny-ImageNet		
		Sym. 20%	Sym. 40%	Sym. 60%	Asym. 40%	Inst. 40%	Sym. 20%	Sym. 50%	Inst. 40%
Standard	ResNet-50	75.5	59.4	41.1	53.4	58.8	68.8	45.9	53.7
SCE	ResNet-50	75.2	69.3	55.2	67.0	57.2	69.7	58.6	67.3
TURN	ResNet-50	80.7	78.6	73.3	69.4	69.8	75.2	71.5	70.6
ELR	ResNet-50	80.9	78.2	73.9	75.6	79.7	70.5	64.2	75.6
CoL	ResNet-50	83.1	81.7	79.2	73.6	80.1	74.9	73.3	74.7
DMix	ResNet-50	84.3	83.1	80.7	66.6	81.3			
UNICON	ResNet-50	84.1	<u>83.2</u>	81.1	76.8	82.1			
DISC	ResNet-50	83.6	82.2	80.1	<u>77.1</u>	<u>82.5</u>	75.7	74.6	75.8
DeFT	CLIP-ResNet-50	<u>84.3</u>	82.9	79.9	64.9	79.3	76.8	73.9	74.1
DODO	ResNet-50	84.9	83.4	<u>81.0</u>	77.8	83.6	78.3	75.3	77.4
SCE	ViT-16/B	91.3	90.4	87.4	73.4	83.6	87.5	86.1	83.2
ELR	ViT-16/B	91.5	90.4	<u>89.7</u>	84.6	<u>91.4</u>	87.2	<u>86.5</u>	<u>87.9</u>
TURN	ViT-16/B	91.0	89.7	88.6	<u>85.1</u>	84.6	86.7	75.3	83.7
DeFT	CLIP-ViT-16/B	<u>92.2</u>	<u>91.2</u>	89.4	72.9	87.6	<u>89.0</u>	72.9	85.2
DODO	ViT-16/B	92.6	92.2	91.3	89.4	91.9	91.0	90.3	90.2

Table 1: Comparison with state-of-the-art LNL algorithms in test accuracy (%) on CIFAR-100 and Tiny-ImageNet datasets. For CIFAR-100, we evaluate symmetric, asymmetric, and instance noise. For Tiny-ImageNet, we evaluate symmetric and instance noise. The best results for each dataset and noise type are highlighted in bold. We report average performance of three random trials for each experiment. The results of all the baseline methods are reproduced using the open-sourced code following *Implements* in Section 5.1.

We further investigate the performance of DODO on three real-world noisy label datasets: **1) CIFAR-100N** [44] ($r \approx 0.4$): A variant of CIFAR-100 with real-world human annotations collected from Amazon Mechanical Turk. **2) Clothing1M** [45] ($r \approx 0.385$): A large-scale dataset consisting of 1 million clothing images across 14 categories, collected from online shopping websites. **3) WebVision** [1] ($r \approx 0.2$): A dataset using 1,000 classes from ImageNet ILSVRC12, containing 2.4 million images crawled from Flickr and Google. Following previous works [8, 22], we conduct experiments on the top 50 classes of the Google image subset.

Architecture and baselines. Using pre-trained models for noise-robust training has been demonstrated to significantly accelerate training speed and enhance training quality [8, 21, 22, 46]. In our experiments, we primarily utilize two widely adopted pre-trained models: ViT-B/16 and ResNet-50. For ResNet-50, we compare DODO with state-of-the-art LNL algorithms, including one-stage methods SCE [47], DivideMix (DMix) [14], ELR [10], Co-learning (CoL) [25], UNICON [16], DISC [12] and two-stage methods TURN [8] and DEFT [22]. However, for ViT-B/16, we compare DODO with SCE, ELR, TURN, and DEFT, without DMix and UNICON. They train two networks simultaneously, requiring a significant number of feed-forwards for each sample, approximately 4 times and 8 times, respectively [8], limiting their scalability. To further verify the effectiveness of DODO on real-world datasets, we also make comparisons with some state-of-the-art methods including LongReMix [48], and ProMix [49].

Implements. We follow the two-stage setting in TURN and DEFT. We run 5 epochs for stage one to obtain the prior knowledge about *wrong event* for each sample, and run 10 epochs for stage two to fully noise-resistant fine-tune the pre-trained model. For two-stage baselines, we run 5 epochs for stage one (usually obtain a clean set) and run 10 epochs for stage two to fully fine-tune the pre-trained model. For one-stage baselines, we run 15 epochs to fully fine-tune the pre-trained model. For detailed hyperparameter settings with respect to the learning rate, optimizer, and baseline, please refer to Appendix B.

5.2 Performance for Noisy Label Learning

Overall performance on synthetic datasets. Table 1 demonstrates that DODO consistently outperforms competing methods in CIFAR100 and Tiny-ImageNet with an average accuracy of 1.1%, achieving state-of-the-art performance on both large and small models. DODO outperforms DMix and UNICON especially in non-symmetric noise through its instance-level modeling and dynamic optimization. DeFT generally performs well in non-asymmetric noise, but faces challenges in resource-constrained scenarios due to its dependence on CLIP. DISC and ELR perform well in non-symmetric noise in exhibit limited correction capability for symmetric noise, which is typically the most straightforward to rectify. Each baseline has limitations in certain scenarios, while DODO, built on difficulty modeling and dynamic optimization, demonstrates strong adaptability in various types and ratios of noise.

Overall performance on real-world datasets. Table 2 demonstrates that DODO consistently outperforms competing methods in three real-world datasets with an average accuracy of 0.8%, achieving state-of-the-art performance in

Method	Architecture	CIFAR-100N	Clothing1M	WebVision
Standard	ResNet-50	56.8	67.5	77.8
SCE	ResNet-50	61.4	69.6	78.3
ELR	ResNet-50	69.2	70.5	80.1
DMix	ResNet-50	72.9	72.7	<u>81.7</u>
CoL	ResNet-50	71.2	72.0	80.9
UNICON	ResNet-50	73.1	<u>72.8</u>	82.6
DISC	ResNet-50	<u>73.3</u>	72.3	81.3
TURN	ResNet-50	69.5	68.3	79.2
DeFT	CLIP-ResNet-50	65.5	70.4	76.6
DODO	ResNet-50	73.6	73.0	82.6
ELR	ViT-16/B	79.0	68.5	83.9
SCE	ViT-16/B	76.4	69.5	83.2
TURN	ViT-16/B	78.1	70.3	83.5
ELR*	CLIP-ViT-16/B	72.8	72.2	79.3
UNICON*	CLIP-ViT-16/B	77.7	70.4	84.6
LongReMix*	CLIP-ViT-16/B	74.0	70.6	84.9
ProMix*	CLIP-ViT-16/B	76.0	70.7	84.5
DeFT*	CLIP-ViT-16/B	<u>79.1</u>	<u>72.5</u>	<u>85.2</u>
DODO	ViT-16/B	81.4	73.3	86.0

Table 2: Comparison with state-of-the-art LNL algorithms in test accuracy (%) on CIFAR-100N, Clothing1M, WebVision dataset. The best results are highlighted in bold. Results marked with an asterisk (*) are from [22], other baseline results are reproduced using the open-sourced code following Implements in Section 5.1

Architecture	ViT-B/16				ConvNeXt-B			
	Sym. 60%		Inst. 40%		Sym. 60%		Inst. 40%	
Noise	Acc.	Time	Acc.	Time	Acc.	Time	Acc.	Time
Metric	Acc.	Time	Acc.	Time	Acc.	Time	Acc.	Time
DMix	90.9	1558	89.5	1596	91.0	3150	88.5	3197
DODO	91.3	443	91.9	458	90.8	779	90.8	785

Table 3: Comparison of methods scalability, running DMix and DODO with larger models ViT-B/16 and ConvNeXt-B on the A100 40GB GPU. We record the accuracy (%) and average training time (sec) per epoch.

both large and small models. DeFT achieves promising results with dual-prompt technique but faces challenges in resource-constrained scenarios due to its dependence on CLIP. DMix and UNICON achieve competitive results in three datasets through dual-network subset partitioning, but with slower training efficiency and limitations in scalability. In challenging real-world noisy scenarios, loss regularization methods, i.e. SCE and ELR, do not perform well because they don't attempt to modify the noisy labels.

5.3 Further Analysis

We also conduct extensive experiments to validate the superiority of the wrong event metric, the effectiveness, efficiency, and scalability of the proposed optimization framework.

Efficiency and scalability of DODO. Existing methods have two drawbacks: high memory demand and low computation efficiency. For instance, DMix and UNICON train two networks simultaneously, which consumes large memory and limits scalability. Moreover, each sample requires 4 to 8 feed-forwards computations, resulting in low efficiency. DODO, in contrast, only requires training a single network by using *wrong event* metric, which can be scaled to larger models. Additionally, each sample only needs two forward computations, achieving higher efficiency. Fig.4 shows that DODO achieves state-of-the-art performance while achieving high efficiency. Table 3 shows DODO performs better on average and nearly 4 times faster than DMix on ViT-B/16 and ConvNeXt-B.

Wrong event VS. other metrics. We adjust the BMM fitting distributions of different metrics to compare their performance in noise modeling. We evaluate the modeling ability of different metrics at different training stages by changing the duration of stage 1. The results are presented in Table 4. Loss shows optimal performance in the **proper** early stage; however, performance rapidly degrades in later stages due to noise overfitting. Although the EMA-loss (Exponential Moving Average loss) slows the speed of noise overfitting in later phases, it concurrently restricts the model's ability to distinguish noisy samples during the initial phase. Both *forgetting event* (FE) and *First k-epoch Learning* (FkL) maintain their ability to identify noise after the model begins to overfit the noise. However, these metrics need to accumulate over time to show noticeable differences, resulting in suboptimal performance in the early stages. Overall, *wrong event* exhibits superior noise modeling capabilities in all training stages. The experiment results align with our theoretical analysis in Section, confirming the exceptional efficacy of *wrong event* in noise identification.

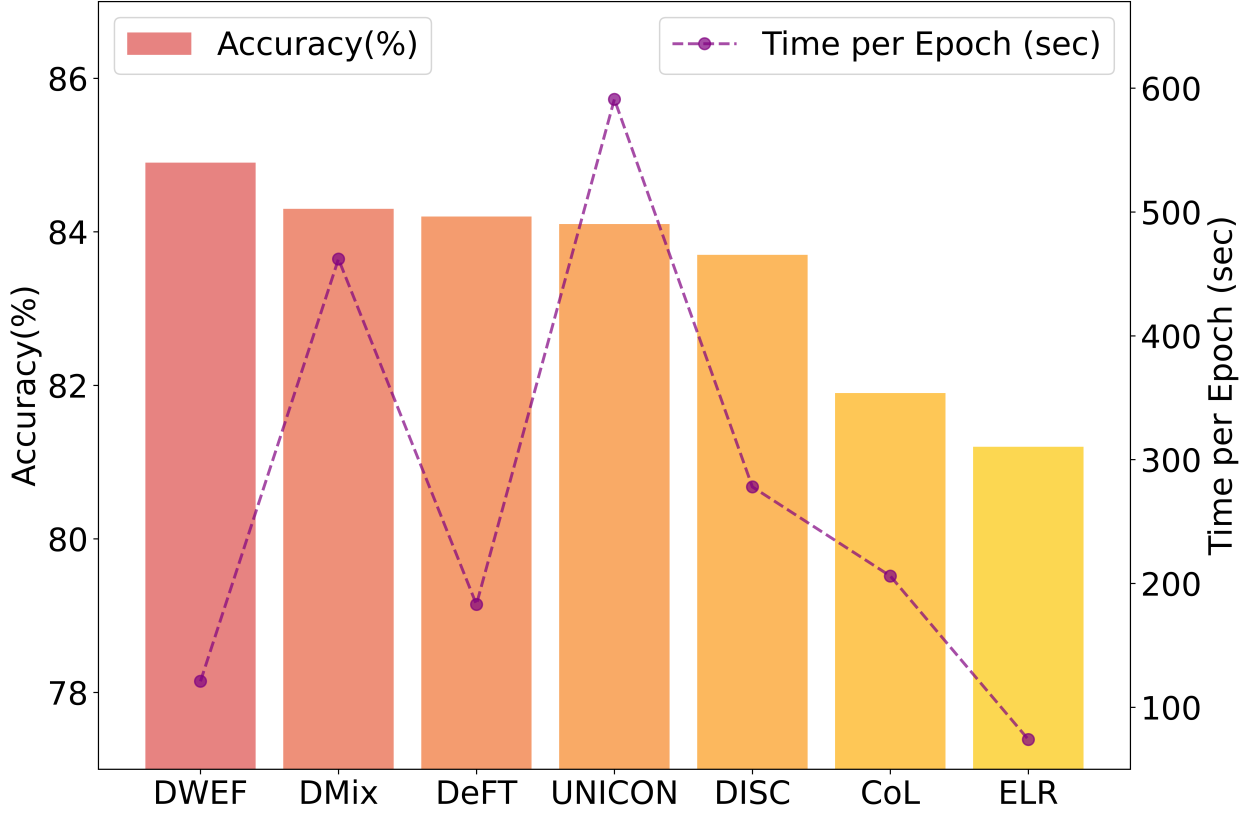


Figure 4: Comparison with state-of-the-art LNL algorithms in effectiveness and efficiency, utilizing pre-trained ResNet50 on the A100 40GB GPU and CIFAR-100 dataset with 20% symmetric noise.

Noise	Sym. 60%					Inst. 40%				
	1	2	4	8	16	1	2	4	8	16
Single Loss	80.2	81.1	<u>79.5</u>	76.3	73.2	<u>78.2</u>	<u>76.9</u>	74.6	68.8	63.2
EMA Loss	79.9	80.9	79.3	77.9	74.9	77.8	74.5	73.6	69.8	64.5
FkL	-	71.8	73.2	78.2	79.6	-	72.9	<u>75.2</u>	80.2	80.5
FE	-	65.8	71.9	75.8	78.9	-	67.0	73.2	81.7	<u>80.8</u>
Wrong Event	80.2	80.9	80.4	79.6	<u>79.1</u>	82.7	83.6	82.6	81.2	80.9

Table 4: Comparison of noise modeling ability across five metrics at four training stages in phase 1, utilizing pre-trained ResNet50 on the CIFAR100 dataset with two noise settings. The training duration for phase 2 was set to 6 epochs by default. The '-' notation indicates cases where BMM fails to provide adequate fitting, due to all samples being assigned an identical metric value of 0.

	Loss Modules			CIFAR100		
	\mathcal{L}_C	\mathcal{L}_N	$\mathcal{L}_{S\mathcal{I}\mathcal{M}}$	Sym. 60%	Asym. 40%	Inst. 40%
✓				75.1	57.7	70.5
✓	✓			<u>79.5</u>	70.4	77.3
✓		✓		78.2	<u>72.0</u>	80.3
✓	✓	✓		81.0	77.8	83.6

Table 5: Ablation studies on the loss modules were conducted using ResNet50 under three different noise settings on CIFAR100.

The effect of different loss term. Our loss function consists of three components: \mathcal{L}_C , \mathcal{L}_N and $\mathcal{L}_{S\mathcal{I}\mathcal{M}}$, modeling clean samples, noisy samples, and difficult samples, respectively. Our ablation experiments demonstrate that all three components contribute to improving the model performance (see Table 5). We observe that \mathcal{L}_N provides higher improvement for symmetric noise, leveraging the accuracy of model outputs to enhance classification performance. On

the other hand, \mathcal{L}_{STM} shows more significant improvements for asymmetric and instance noise, improving the model ability to learn from difficult samples by enforcing consistency in predictions.

A More Empirical Observation of Wrong Event

We show a comparison between wrong event and loss under symmetric noise (see Fig.1). We also conduct experiments under asymmetric noise, and instance-dependent noise to verify that *wrong event* outperforms the loss across all types of noise. Fig.5 and Fig.6 show a comparison between wrong event and loss under asymmetric noise and instance noise, respectively. The experiment results reveal that in more challenging noisy environments, the model tends to rapidly fit the loss of noisy samples, resulting in compromised accuracy and stability of the provided modeling information. In contrast, the wrong event metric maintains its capability to deliver robust modeling information regarding sample cleanliness and difficulty.

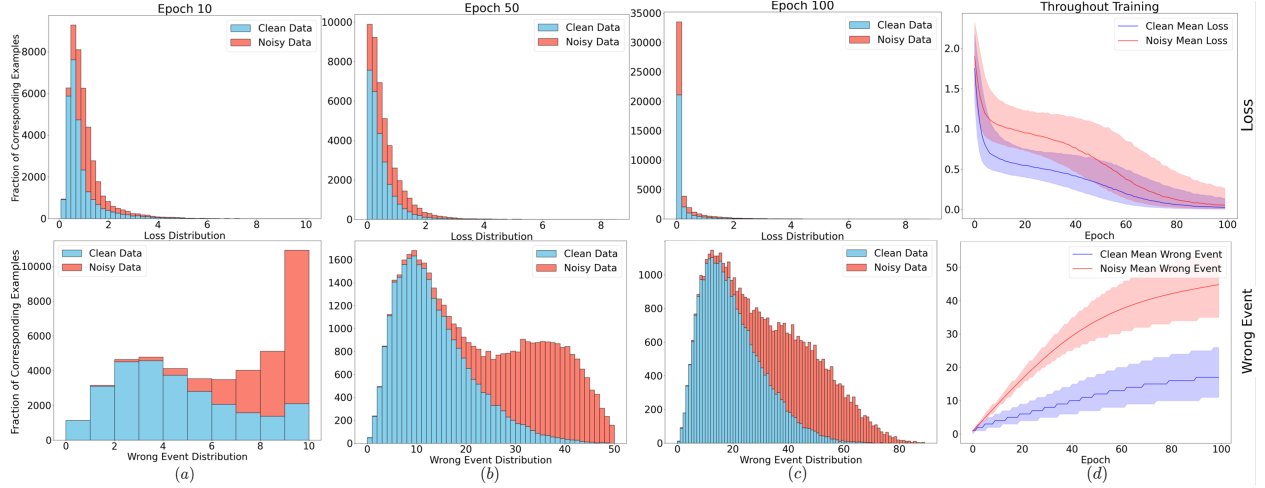


Figure 5: A comparison between wrong event and loss. The baseline model is ResNet-18 trained on CIFAR-10 with 40% asymmetric noise for 100 epochs. We show the loss distributions (upper row) and wrong event distribution (lower row) during training. The four columns, (a) (b) (c) (d), represent the distributions at epoch 10, 50, 100 and during the entire training phase where the heavy lines represent the median value and the shaded areas are the interquartile ranges, respectively. It can be seen that wrong event can clearly separate noisy data and clean data, even if the model fits noise.

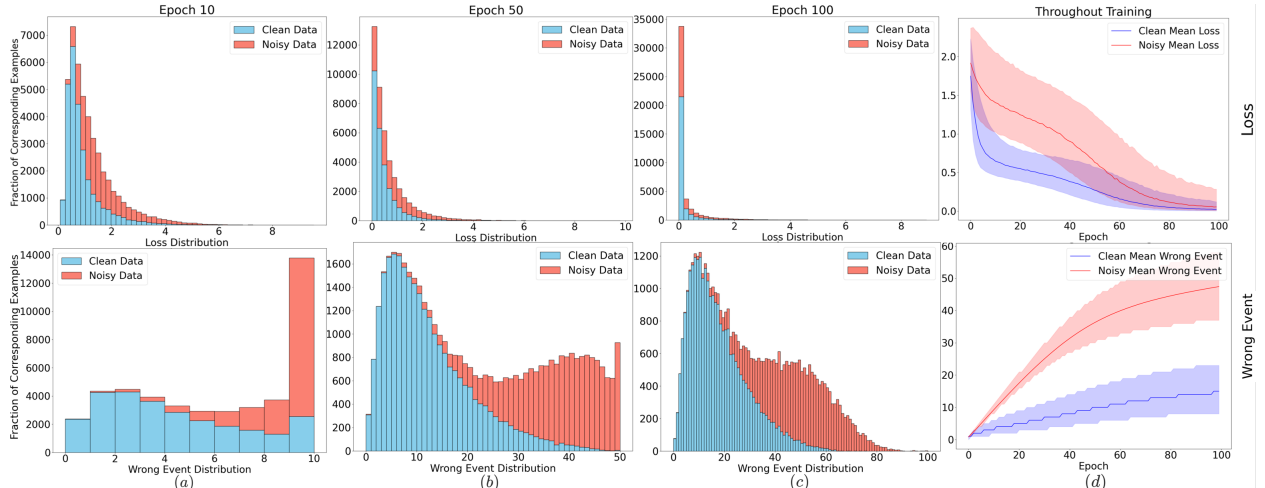


Figure 6: A comparison between wrong event and loss. The baseline model is ResNet-18 trained on CIFAR-10 with 40% instance noise for 100 epochs. We show the loss distributions (upper row) and wrong event distribution (lower row) during training. The four columns, (a) (b) (c) (d), represent the distributions at epoch 10, 50, 100 and during the entire training phase where the heavy lines represent the median value and the shaded areas are the interquartile ranges, respectively. It can be seen that wrong event can clearly separate noisy data and clean data, even if the model fits noise.

B Additional Implementation Details

Regarding the hyperparameters of the model. In our experiments, we primarily utilized pre-trained ResNet-50 and ViT-16/B models, both of which were obtained by calling the PyTorch timm library. For the pre-training hyperparameters of the model, we adhered to the settings used in prior work [8, 22], as detailed in Table 6. One-stage baselines follow the setting in stage 2.

Phase	Stage 1			Stage 2		
	ViT-B/16	ResNet-50	ConvNeXt-B	ViT-B/16	ResNet-50	ConvNeXt-B
Optimizer	SGD	AdamW	AdamW	SGD	AdamW	AdamW
Learning Rate	1×10^{-2}	1×10^{-3}	1×10^{-4}	1×10^{-2}	1×10^{-3}	1×10^{-4}
Weight Decay	1×10^{-5}	1×10^{-5}	1×10^{-4}	1×10^{-5}	1×10^{-5}	1×10^{-4}
Scheduler Strategies	No LP	No FFT	No LP	Cosine FFT	Cosine FFT	Cosine FFT

Table 6: Optimizer configurations for different models and stages.

Regarding the details of the datasets. For synthetic datasets, we added noise to the entire training set and used the test set to evaluate performance. The model quality was determined by the accuracy on the test set at the last epoch. CIFAR100 consists of 100 classes, with 50,000 training images and 10,000 test images, and we set the batch size to 128. Tiny-ImageNet contains 200 classes, with 100,000 training images and 10,000 test images, and we also set the batch size to 128. For real-world datasets, we only used the noisy datasets and did not utilize the clean subsets provided by the datasets. Clothing1M is a class-imbalanced dataset, and we randomly sampled class-balanced subsets each time, with a batch size of 64 and 1,000 iterations. CIFAR100N is identical to CIFAR100 except for its real-world noisy labels. For WebVision, we used the first 50 classes, which include 66000 training images and 2,500 test images, and we set the batch size to 128.

Regarding the hyperparameters of the baselines. The baseline results were generated under consistent experimental settings using publicly available code. The hyperparameters were configured according to the recommendations outlined in the original papers.

SCE [47] is a robust noise-tolerant loss function with two hyperparameters, α and β . The original paper suggests that a large α may lead to overfitting, while a small α can mitigate overfitting but slow down convergence. Therefore, the authors recommend using a small α and a large β to replace existing loss functions. Since pre-trained models converge faster, we adopted the configuration proposed in the original paper to suppress overfitting to noise, setting $\alpha = 0.1, \beta = 1$.

ELR [10] introduces a regularization term to the loss function, leveraging the correct predictions of noisy samples during early learning to achieve noise-robust learning with two hyperparameters, λ and β . The authors recommend hyperparameter settings of CIFAR100, Clothing1M and WebVision, with $\lambda = 3, \beta = 0.7$. We applied the same settings across these datasets. For CIFAR100N and Tiny-ImageNet, we adopted the same configuration as used for CIFAR100.

DivideMix [14] is a co-training-based label correction method that introduces five key hyperparameters: number of MixMatch views M , temperature of sharpen labels T , mixup parameter α , GMM threshold τ and unsupervised loss term coefficient λ_u . We followed the original paper’s settings, for most experiments, setting $M = 2, T = 0.5, \alpha = 4, \tau = 0.5$, and $\lambda_u = 50$.

Co-learning [25] is a method combining supervised learning and self-supervised learning, with $L = L_{sup} + L_{int} + L_{str}$. All the coefficients of loss terms are set to 1 following the original paper.

UNICON [16] is a co-training-based label correction method that combines supervised learning, semi-supervised learning and contrastive learning. There are seven main parameters mentioned: unsupervised loss coefficient λ_u , regularization coefficient λ_r , contrastive loss coefficient λ_C , filter coefficient τ , adjustment threshold d_μ and mixup coefficient α . Following the original paper, we set $\lambda_C = 0.025, \lambda_u = 30, \lambda_r = 1, d_\mu = 0.7, \tau = 5$ and $\alpha = 4$.

DISC [12] is a method which dynamically selects and corrects dataset. Four main hyperparameters are mentioned: warm-up period T_0 , coefficient of the hard-set loss λ_h , momentum coefficient λ and positive offset value σ . Following the pre-trained model setting in the original paper, we set $T_0 = 1, \lambda = 0.7, \lambda_h = 0.2$ and $\sigma = 0.3$.

Hyperparameter	regularization term weight λ						momentum coefficient β						DODO
	0	1	3	5	7	10	0.1	0.3	0.5	0.7	0.9	0.99	
Noise Dataset	0	1	3	5	7	10	0.1	0.3	0.5	0.7	0.9	0.99	
CIFAR-100 Sym. 60%	41.1	41.7	73.9	75.9	46.4	1.0	12.2	75.9	77.1	73.9	51.3	42.9	80.9
CIFAR-100 Inst. 40%	58.8	56.0	79.7	82.9	69.5	25.0	49.9	82.9	82.6	79.7	67.3	59.4	83.6
CIFAR-100N	61.0	61.6	69.2	68.8	62.7	9.1	56.1	70.7	71.8	69.2	65.3	62.1	73.6

Table 7: Hyperparameter sensitivity of ELR, utilizing pre-trained ResNet50 on the CIFAR100 dataset with three noise settings. The default values are set as $\lambda = 3$ and $\beta = 0.7$. We consider the value ranges of $\lambda \in \{0, 1, 3, 5, 7, 10\}$ and $\beta \in \{0.1, 0.3, 0.5, 0.7, 0.9, 0.99\}$. following the discussion in original paper [10]

Hyperparameter	\mathcal{L}_u term weight λ_u				GMM threshold τ					Mixup parameter α				DODO
	0	25	50	150	0.1	0.3	0.5	0.7	0.9	0.5	1	2	4	
Noise Dataset	0	25	50	150	0.1	0.3	0.5	0.7	0.9	0.5	1	2	4	
CIFAR-100 Sym. 60%	80.7	79.3	79.9	80.8	81.1	80.5	79.6	67.4	29.8	80.9	79.7	79.2	78.0	80.9
CIFAR-100 Inst. 40%	79.7	79.9	81.9	81.1	80.3	79.3	79.7	78.1	70.5	79.8	81.1	82.3	81.3	83.6
CIFAR-100 Asym. 40%	63.2	63.6	66.6	67.9	63.8	65.3	66.6	65.9	57.6	60.3	62.1	66.4	66.6	77.8

Table 8: Hyperparameter sensitivity of DivideMix, utilizing pre-trained ResNet50 on the CIFAR100 dataset with three noise settings. The default values are set as $\lambda_u = 50$, $\tau = 0.5$ and $\alpha = 4$. We consider the value ranges of $\lambda_u \in \{0, 25, 50, 150\}$, $\tau \in \{0.1, 0.3, 0.5, 0.7, 0.9\}$ and $\alpha \in \{0.5, 1, 2, 4\}$ following the discussion in original paper [14].

TURN [8] is a method which firstly uses noise-robust loss function to obtain a clean set with LP, and FFT the model on the clean set. The main hyperparameter is the GMM threshold τ . Following the original paper, we set $\tau = 0.6$ in all experiments.

DeFT [22] is a CLIP-based method which used dual prompts on CLIP to obtain a clean set with parameter-efficient fine-tuning (PEFT), and FFT the pre-trained downstream model on the clean set. The heavy reliance on CLIP significantly limits the method’s applicability in computational resource-constrained scenarios.

C Sensitivity Analysis of Parameter Configurations in Two Advanced Methods

In this section, we conduct comprehensive experiments on two advanced algorithms, ELR [10] and DMix [14], to investigate the sensitivity of manually fixed parameters. Our analysis focuses on key hyperparameters including the subset division threshold, loss term weights, momentum averaging coefficients, among others.

C.1 Analysis and Experiments of ELR

ELR algorithm incorporates two crucial hyperparameters: the regularization term weight λ and the temporal ensembling momentum coefficient β . Table 7 demonstrates the parameter sensitivity of ELR, showing that the performance is significantly influenced by parameter choices and comparison with the result of DODO. The parameter settings recommended for training from scratch in the original paper, where the authors recommend $\beta = 0.7$, $\lambda = 3$ for symmetric noise on CIFAR100 and $\beta = 0.9$, $\lambda = 7$ for asymmetric noise on CIFAR-100. However, parameter settings undergo significant shifts in pretrained settings. Optimal performance is achieved when $\beta \in [0.3, 0.5]$, $\lambda \in [3, 5]$, demonstrating that optimal hyperparameters vary across different models and datasets, necessitating careful parameter tuning. Our proposed method DODO effectively addresses this challenge through dynamically weighted optimization.

C.2 Analysis and Experiments of DivideMix

DivideMix algorithm incorporates three crucial hyperparameters: the unsupervised loss term weight λ_u , GMM threshold τ for subset partitioning and beta distribution parameter α of Mixup [50]. Table 8 demonstrates the parameter sensitivity of DivideMix, showing that the performance is significantly influenced by parameter choices and comparison with DODO’s result. The parameter settings recommended for training from scratch in the original paper, where the authors recommend $\lambda_u = 25$, $\tau \in [0.5, 0.6]$, $\alpha = 4$ for symmetric noise on CIFAR100 and $\lambda_u = 0$, $\tau = 0.5$, $\alpha = 4$ for asymmetric noise on CIFAR-100. However, parameter settings undergo significant shifts in pretrained settings. Optimal performance is achieved when $\lambda_u \in [50, 150]$, $\tau \in [0.1, 0.5]$ shows that optimal hyperparameters vary between different

models and data sets, which requires careful parameter tuning. Our proposed method DODO effectively addresses this challenge through dynamically weighted optimization.

References

- [1] Wen Li, Limin Wang, Wei Li, Eirikur Agustsson, and Luc Van Gool. Webvision database: Visual learning and understanding from web data. *arXiv preprint arXiv:1708.02862*, 2017.
- [2] Yan Yan, Rómer Rosales, Glenn Fung, Ramanathan Subramanian, and Jennifer Dy. Learning from multiple annotators with varying expertise. *Machine Learning*, 95(3):291–327, 2014.
- [3] C. Fabian Benitez-Quiroz, Ramprakash Srinivasan, and Aleix M. Martinez. Emotionet: An accurate, real-time algorithm for the automatic annotation of a million facial expressions in the wild. In *Proc. CVPR*, pages 5562–5570, 2016.
- [4] Chiyuan Zhang, Samy Bengio, Moritz Hardt, Benjamin Recht, and Oriol Vinyals. Understanding deep learning requires rethinking generalization. In *International Conference on Learning Representations*, 2017.
- [5] Devansh Arpit, Stanisław Jastrzębski, Nicolas Ballas, David Krueger, Emmanuel Bengio, Maxinder S. Kanwal, Tegan Maharaj, Asja Fischer, Aaron Courville, and Yoshua Bengio et al. A closer look at memorization in deep networks. In *Proc. ICML*, pages 233–242, 2017.
- [6] Bo Han, Quanming Yao, Xingrui Yu, Gang Niu, Miao Xu, Weihua Hu, Ivor Tsang, and Masashi Sugiyama. Co-teaching: Robust training of deep neural networks with extremely noisy labels. In *Proc. NeurIPS*, volume 31, 2018.
- [7] Jinchi Huang, Lie Qu, Rongfei Jia, and Binqiang Zhao. O2u-net: A simple noisy label detection approach for deep neural networks. In *2019 IEEE/CVF International Conference on Computer Vision (ICCV)*, pages 3325–3333, 2019.
- [8] Sumyeong Ahn, Sihyeon Kim, Jongwoo Ko, and Se-Young Yun. Fine-tuning pre-trained models for robustness under noisy labels. In *Proceedings of the Thirty-Third International Joint Conference on Artificial Intelligence, IJCAI-24*, pages 3643–3651, 8 2024.
- [9] Eric Arazo, Diego Ortego, Paul Albert, Noel O’Connor, and Kevin McGuinness. Unsupervised label noise modeling and loss correction. In *Proceedings of the 36th International Conference on Machine Learning*, volume 97 of *Proceedings of Machine Learning Research*, pages 312–321, 2019.
- [10] Sheng Liu, Jonathan Niles-Weed, Narges Razavian, and Carlos Fernandez-Granda. Early-learning regularization prevents memorization of noisy labels. In *Proc. NeurIPS*, volume 33, pages 20331–20342, 2020.
- [11] Xichen Ye, Xiaoqiang Li, Songmin Dai, Tong Liu, Yan Sun, and Weiqin Tong. Active negative loss functions for learning with noisy labels. In *Thirty-seventh Conference on Neural Information Processing Systems*, 2023.
- [12] Yifan Li, Hu Han, Shiguang Shan, and Xilin Chen. Disc: Learning from noisy labels via dynamic instance-specific selection and correction. In *Proceedings of the IEEE/CVF Conference on Computer Vision and Pattern Recognition*, pages 24070–24079, 2023.
- [13] Sheng Guo, Weilin Huang, Haozhi Zhang, Chenfan Zhuang, Dengke Dong, Matthew R. Scott, and Dinglong Huang. Curriculumnet: Weakly supervised learning from large-scale web images. In Vittorio Ferrari, Martial Hebert, Cristian Sminchisescu, and Yair Weiss, editors, *Computer Vision – ECCV 2018*, 2018.
- [14] Junnan Li, Richard Socher, and Steven C. H. Hoi. Dividemix: Learning with noisy labels as semi-supervised learning. In *Proc. ICLR*, 2019.
- [15] Xuefeng Liang, Longshan Yao, Xingyu Liu, and Ying Zhou. Tripartite: Tackle noisy labels by a more precise partition. *ArXiv*, abs/2202.09579, 2022.
- [16] Nazmul Karim, Mamshad Nayeem Rizve, Nazanin Rahnavard, Ajmal Mian, and Mubarak Shah. Unicon: Combating label noise through uniform selection and contrastive learning. In *2022 IEEE/CVF Conference on Computer Vision and Pattern Recognition (CVPR)*, pages 9666–9676, 2022.
- [17] Ziyi Zhang, Weikai Chen, Chaowei Fang, Zhen Li, Lechao Chen, Liang Lin, and Guanbin Li. Rankmatch: Fostering confidence and consistency in learning with noisy labels. In *2023 IEEE/CVF International Conference on Computer Vision (ICCV)*, pages 1644–1654, 2023.
- [18] Tianyi Zhou, Shengjie Wang, and Jeff Bilmes. Robust curriculum learning: from clean label detection to noisy label self-correction. In *International Conference on Learning Representations*, 2021.

[19] Mariya Toneva, Alessandro Sordoni, Remi Tachet des Combes, Adam Trischler, Yoshua Bengio, and Geoffrey J. Gordon. An empirical study of example forgetting during deep neural network learning. In *International Conference on Learning Representations*, 2019.

[20] Suqin Yuan, Lei Feng, and Tongliang Liu. Late stopping: Avoiding confidently learning from mislabeled examples. 2023 IEEE/CVF International Conference on Computer Vision (ICCV), pages 16033–16042, 2023.

[21] Evgenii Zheltonozhskii, Chaim Baskin, Avi Mendelson, Alex M. Bronstein, and Or Litany. Contrast to Divide: Self-Supervised Pre-Training for Learning with Noisy Labels . In 2022 IEEE/CVF Winter Conference on Applications of Computer Vision (WACV), pages 387–397, 2022.

[22] Tong Wei, Hao-Tian Li, Chun-Shu Li, Jiang-Xin Shi, Yu-Feng Li, and Min-Ling Zhang. Vision-language models are strong noisy label detectors. In *The Thirty-eighth Annual Conference on Neural Information Processing Systems*, 2024.

[23] Or Litany and Daniel Freedman. SOSELETO: A unified approach to transfer learning and training with noisy labels, 2019.

[24] Guoqing Zheng, Ahmed Hassan Awadallah, and Susan T. Dumais. Meta label correction for noisy label learning. In *AAAI Conference on Artificial Intelligence*, 2021.

[25] Cheng Tan, Jun Xia, Lirong Wu, and Stan Z. Li. Co-learning: Learning from noisy labels with self-supervision. In *Proceedings of the 29th ACM International Conference on Multimedia*, page 1405–1413, 2021.

[26] Alexey Dosovitskiy, Lucas Beyer, Alexander Kolesnikov, Dirk Weissenborn, Xiaohua Zhai, Thomas Unterthiner, Mostafa Dehghani, Matthias Minderer, Georg Heigold, Sylvain Gelly, Jakob Uszkoreit, and Neil Houlsby. An image is worth 16x16 words: Transformers for image recognition at scale. In *International Conference on Learning Representations*, 2021.

[27] Alec Radford, Jong Wook Kim, Chris Hallacy, Aditya Ramesh, Gabriel Goh, Sandhini Agarwal, Girish Sastry, Amanda Askell, Pamela Mishkin, Jack Clark, Gretchen Krueger, and Ilya Sutskever. Learning transferable visual models from natural language supervision. In *International Conference on Machine Learning*, 2021.

[28] Shikun Li, Xiaobo Xia, Shimeng Ge, and Tongliang Liu. Selective-supervised contrastive learning with noisy labels. 2022 IEEE/CVF Conference on Computer Vision and Pattern Recognition (CVPR), pages 316–325, 2022.

[29] Ting Chen, Simon Kornblith, Mohammad Norouzi, and Geoffrey Hinton. A simple framework for contrastive learning of visual representations. In *Proceedings of the 37th International Conference on Machine Learning*. JMLR.org, 2020.

[30] Kaiming He, Haoqi Fan, Yuxin Wu, Saining Xie, and Ross Girshick. Momentum contrast for unsupervised visual representation learning. In 2020 IEEE/CVF Conference on Computer Vision and Pattern Recognition (CVPR), pages 9726–9735, 2020.

[31] Chen Feng, Georgios Tzimiropoulos, and Ioannis Patras. Clipcleaner: Cleaning noisy labels with clip. In *Proceedings of the 32nd ACM International Conference on Multimedia*, page 876–885, New York, NY, USA, 2024. Association for Computing Machinery.

[32] Kaiming He, Xiangyu Zhang, Shaoqing Ren, and Jian Sun. Deep residual learning for image recognition. In 2016 IEEE Conference on Computer Vision and Pattern Recognition (CVPR), pages 770–778, 2016.

[33] Zhuang Liu, Hanzi Mao, Chao-Yuan Wu, Christoph Feichtenhofer, Trevor Darrell, and Saining Xie. A convnet for the 2020s. In 2022 IEEE/CVF Conference on Computer Vision and Pattern Recognition (CVPR), pages 11966–11976, 2022.

[34] Suqin Yuan, Lei Feng, and Tongliang Liu. Early stopping against label noise without validation data. In *The Twelfth International Conference on Learning Representations*, 2024.

[35] Tsung-Yi Lin, Priya Goyal, Ross Girshick, Kaiming He, and Piotr Dollár. Focal loss for dense object detection. In 2017 IEEE International Conference on Computer Vision (ICCV), pages 2999–3007, 2017.

[36] Buyu Li, Yu Liu, and Xiaogang Wang. Gradient harmonized single-stage detector. In *Proceedings of the Thirty-Third AAAI Conference on Artificial Intelligence and Thirty-First Innovative Applications of Artificial Intelligence Conference and Ninth AAAI Symposium on Educational Advances in Artificial Intelligence*, AAAI’19/IAAI’19/EAAI’19. AAAI Press, 2019.

[37] Yoshua Bengio, Jérôme Louradour, Ronan Collobert, and Jason Weston. Curriculum learning. In *Proceedings of the 26th Annual International Conference on Machine Learning*, ICML ’09, page 41–48, 2009.

[38] Zhanyu Ma and Arne Leijon. Bayesian estimation of beta mixture models with variational inference. *IEEE Transactions on Pattern Analysis and Machine Intelligence*, 33(11):2160–2173, 2011.

- [39] Kento Nishi, Yi Ding, Alex Rich, and Tobias Hollerer. Augmentation strategies for learning with noisy labels. In *Proceedings of the IEEE/CVF Conference on Computer Vision and Pattern Recognition (CVPR)*, pages 8022–8031, June 2021.
- [40] Junnan Li, Caiming Xiong, and Steven C.H. Hoi. Learning from noisy data with robust representation learning. In *2021 IEEE/CVF International Conference on Computer Vision (ICCV)*, pages 9465–9474, 2021.
- [41] Alex Krizhevsky. Learning multiple layers of features from tiny images. 2009.
- [42] Jiayu Wu, Qixiang Zhang, and Guoxi Xu. Tiny imagenet challenge. Technical report, 2017.
- [43] Xiaobo Xia, Tongliang Liu, Bo Han, Nannan Wang, Mingming Gong, Haifeng Liu, Gang Niu, Dacheng Tao, and Masashi Sugiyama. Part-dependent label noise: Towards instance-dependent label noise. *Advances in Neural Information Processing Systems*, 33:7597–7610, 2020.
- [44] Jiaheng Wei, Zhaowei Zhu, Hao Cheng, Tongliang Liu, Gang Niu, and Yang Liu. Learning with noisy labels revisited: A study using real-world human annotations. In *International Conference on Learning Representations*, 2022.
- [45] Tong Xiao, Tian Xia, Yi Yang, Chang Huang, and Xiaogang Wang. Learning from massive noisy labeled data for image classification. In *Proceedings of the IEEE Conference on Computer Vision and Pattern Recognition (CVPR)*, 2015.
- [46] Jongwoo Ko, Sumyeong Ahn, and Se-Young Yun. EFFICIENT UTILIZATION OF PRE-TRAINED MODEL FOR LEARNING WITH NOISY LABELS. In *ICLR 2023 Workshop on Pitfalls of limited data and computation for Trustworthy ML*, 2023.
- [47] Yisen Wang, Xingjun Ma, Zaiyi Chen, Yuan Luo, Jinfeng Yi, and James Bailey. Symmetric cross entropy for robust learning with noisy labels. In *2019 IEEE/CVF International Conference on Computer Vision (ICCV)*, pages 322–330, 2019.
- [48] Filipe R. Cordeiro, Ragav Sachdeva, Vasileios Belagiannis, Ian Reid, and Gustavo Carneiro. Longremix: Robust learning with high confidence samples in a noisy label environment. *Pattern Recognition*, 133:109013, 2023.
- [49] Ruixuan Xiao, Yiwen Dong, Haobo Wang, Lei Feng, Runze Wu, Gang Chen, and Junbo Zhao. Promix: Combating label noise via maximizing clean sample utility. In Edith Elkind, editor, *Proceedings of the Thirty-Second International Joint Conference on Artificial Intelligence, IJCAI-23*, pages 4442–4450, 8 2023.
- [50] Hongyi Zhang, Moustapha Cisse, Yann N. Dauphin, and David Lopez-Paz. mixup: Beyond empirical risk minimization. In *International Conference on Learning Representations*, 2018.